Incomplete proteasomal degradation of green fluorescent proteins in the context of tandem fluorescent protein timers

Anton Khmelinskii, Matthias Meurer, Chi-Ting Ho, Birgit Besenbeck, Julia Füller, Marius K. Lemberg, Bernd Bukau, Axel Mogk, and Michael Knop
Zentrum für Molekulare Biologie der Universität Heidelberg and Deutsches Krebsforschungszentrum, DKFZ-ZMBH Alliance, 69120 Heidelberg, Germany

ABSTRACT **Tandem fluorescent protein timers (tFTs) report on protein age through time-dependent change in color, which can be exploited to study protein turnover and trafficking. Each tFT, composed of two fluorescent proteins (FPs) that differ in maturation kinetics, is suited to follow protein dynamics within a specific time range determined by the maturation rates of both FPs. So far, tFTs have been constructed by combining slower-maturing red fluorescent proteins (redFPs) with the faster-maturing superfolder green fluorescent protein (sfGFP). Toward a comprehensive characterization of tFTs, we compare here tFTs composed of different faster-maturing green fluorescent proteins (greenFPs) while keeping the slower-maturing redFP constant (mCherry). Our results indicate that the greenFP maturation kinetics influences the time range of a tFT. Moreover, we observe that commonly used greenFPs can partially withstand proteasomal degradation due to the stability of the FP fold, which results in accumulation of tFT fragments in the cell. Depending on the order of FPs in the timer, incomplete proteasomal degradation either shifts the time range of the tFT toward slower time scales or precludes its use for measurements of protein turnover. We identify greenFPs that are efficiently degraded by the proteasome and provide simple guidelines for the design of new tFTs.**

Monitoring Editor
Mark J. Solomon
Yale University

Received: Jul 23, 2015
Revised: Nov 12, 2015
Accepted: Nov 16, 2015

INTRODUCTION

Fluorescent proteins (FPs) become fluorescent only upon correct folding of the polypeptide and formation of the fluorophore through a series of chemical reactions within the β-barrel fold. This maturation process takes place on time scales from minutes to hours, depending on the FP and the environment (Tsien, 1998; Shaner *et al.*, 2005). The time delay between protein synthesis and completion of the maturation process is exploited in tandem fluorescent protein timers (tFTs) to measure the dynamics of various cellular processes (Khmelinskii *et al.*, 2012). A tFT is a fusion of two FPs that differ in maturation kinetics and spectral properties (i.e., color)—for example, a slower-maturing red fluorescent protein (redFP) and a faster-maturing green fluorescent protein (greenFP; Figure 1A). The greenFP is typically selected to be as rapidly maturing as possible and thus reports on protein localization and abundance. Because of the difference in maturation kinetics between the greenFP and redFP moieties, the color of a tFT (defined as the redFP/greenFP ratio of fluorescence intensities) changes over time (Figure 1A). When a tFT is fused to a protein of interest, its color provides a measure of protein age that can be used to follow protein degradation, trafficking, and segregation during cell division (Khmelinskii *et al.*, 2012).

The range of protein ages that can be analyzed with a tFT, that is, its time range, is strongly influenced by the maturation kinetics of the slower-maturing FP in the pair (Khmelinskii *et al.*, 2012). Therefore, in the tFTs described thus far (Khmelinskii *et al.*, 2012; Khmelinskii and Knop, 2014; Dona *et al.*, 2013), different slower-maturing redFPs (mCherry, TagRFP, DsRed1) were combined with the same faster-maturing greenFP (superfolder green fluorescent protein [sfGFP]; Pédelacq *et al.*, 2006). Several properties make sfGFP a greenFP of choice for construction of tFTs: it is bright, it

This article was published online ahead of print in MBoC in Press (http://www.molbiolcell.org/cgi/doi/10.1091/mbc.E15-07-0525) on November 25, 2015.
Address correspondence to: M. Knop (m.knop@zmbh.uni-heidelberg.de).
Abbreviations used: FP, fluorescent protein; GFP, greenFP, green fluorescent protein; RFP, redFP, red fluorescent protein; tFT, tandem fluorescent protein timer.

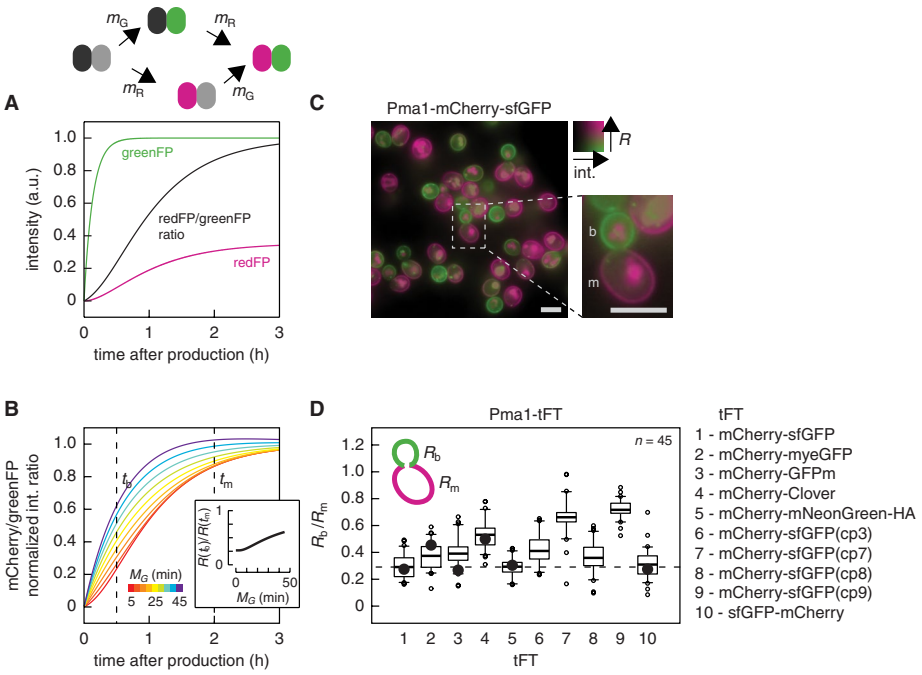

FIGURE 1: Analysis of protein age with different tFTs. (A) Behavior of a tFT composed of a slower-maturing redFP (black-magenta, maturation rate constant m_R) and a faster-maturing greenFP (gray-green, maturation rate constant m_G). Fluorescence intensity curves were calculated using published maturation parameters for mCherry (redFP) and sfGFP (greenFP) for a population of tFT molecules initialized in the nonmature state in the absence of protein production and degradation (Khmelinskii *et al.*, 2012). Intensity curves are normalized to the brightness of sfGFP, and the ratio curve is normalized to the point of complete maturation. (B) tFTs composed of mCherry and greenFPs with different maturation kinetics. mCherry/greenFP intensity ratio curves were calculated as in A using published maturation parameters for mCherry (Khmelinskii *et al.*, 2012) and a maturation half-time M_G between 5 and 45 min for greenFP. Note that the maturation half-time is related to the maturation rate constant m_G as $M_G = \ln(2)/m_G$. Each curve is normalized to the point of complete maturation. Curves are color-coded according to M_G as indicated. Inset, comparison of mCherry/greenFP intensity ratio (R) at two time points, $t_b = 30$ min (approximate age of a bud) and $t_m = 2$ h (approximate age of a young mother cell), as a function of M_G. (C) Representative intensity-weighted ratiometric image of cells expressing Pma1-mCherry-sfGFP, color coded according to sfGFP intensity (int.) and mCherry/sfGFP intensity ratio (R). A dividing cell with labeled mother (m) and bud (b) compartments is shown. Scale bars, 5 µm. (D) mCherry/greenFP intensity ratio (R) of Pma1 tagged with the indicated tFTs were measured at the plasma membrane in pairs of mother (R_m) and bud (R_b) cells ($n = 45$ pairs for each tFT). Centerlines mark the medians, box limits indicate the 25th and 75th percentiles, and whiskers extend to 5th and 95th percentiles. The difference between R_m and R_b is significant for all tFTs ($p < 10^{-19}$ in a paired t test). The mCherry-mNeonGreen timer carried a C-terminal hemagglutinin epitope (HA) tag to facilitate detection by immunoblotting. Black circles mark theoretical R_b/R_m values calculated according to a simple model of mCherry-greenFP maturation in B using 30 min and 2 h as approximate ages of a bud and a young mother cell, respectively, and published maturation half-times for mCherry and different greenFPs (Khmelinskii *et al.*, 2012).

folds independently of the protein to which it is fused (Pédelacq *et al.*, 2006), it is one of the faster-maturing greenFPs, with a maturation half-time of ~6 min in yeast (Khmelinskii *et al.*, 2012), and an additional V206R mutation ensures that it is monomeric (Zacharias *et al.*, 2002). Nevertheless, there is a wide range of greenFPs with other desirable properties, such as high molecular brightness or high photostability (Dean and Palmer, 2014). However, their in vivo maturation rates, which determine their suitability for construction of new tFTs (Figure 1B), are not well characterized.

Here we compared the performance of different greenFPs within tFTs. We constructed a series of mCherry-greenFP timers and examined their suitability for comparative measurements of protein age and protein degradation kinetics in yeast. We identified the stability of the greenFP fold as a new parameter that affects tFT behavior and directs the design and use of tFT as reporters of protein degradation.

RESULTS

We constructed new putative tFTs by fusing the slower-maturing redFP mCherry (Shaner *et al.*, 2004) to different greenFPs: the commonly used monomeric, yeast codon-optimized, enhanced GFP (myeGFP; GFPmut 3a from Cormack *et al.* [1996] with a V206R dimerization-preventing mutation [Zacharias *et al.*, 2002]), the fast-maturing GFPm (Yoo *et al.*, 2007; Iizuka *et al.*, 2011), and two greenFPs with superior brightness—Clover (Lam *et al.*, 2012) and mNeonGreen (Shaner *et al.*, 2013; Supplemental Figure S1, A and B). myeGFP, GFPm, Clover, and mNeonGreen have red-shifted excitation peaks compared with sfGFP. Using such greenFPs is likely to improve signal-to-noise ratio in fluorescence imaging, as autofluorescence of yeast cells and growth media is substantially reduced with excitation wavelengths >488 nm (Supplemental Figure S1C).

To test whether these mCherry-greenFP fusions function as timers and compare their ability to report on protein age, we analyzed cells expressing the proton pump Pma1 tagged with each putative tFT. Pma1 is an exceptionally stable protein of the plasma membrane (Thayer *et al.*, 2014). During yeast bud formation, preexisting Pma1 molecules at the plasma membrane are retained in the mother cell, and the bud (future daughter cell) receives newly produced Pma1 (Takizawa *et al.*, 2000; Malínská *et al.*, 2003). Consequently, cells expressing Pma1 tagged with the mCherry-sfGFP timer exhibit a lower mCherry/greenFP intensity ratio (R) at the plasma membrane in the bud (R_b) than in the mother cell (R_m; Figure 1C; Khmelinskii *et al.*, 2012). We observed the same trend for all Pma1 fusions (Figure 1D), indicating that all tested mCherry-greenFP variants function as timers.

The R_b/R_m ratio can be used for a qualitative comparison of greenFP maturation rates with an approximate model of tFT maturation (Figure 1B; Khmelinskii *et al.*, 2012). The R_b/R_m ratio was lowest for mCherry-sfGFP and mCherry-mNeonGreen timers (Figure 1D), indicating that sfGFP and mNeonGreen have the fastest maturation among all tested greenFPs. Consistent with slower maturation of Clover (Supplemental Figure S1A), the R_b/R_m ratio was highest for the strain expressing Pma1-mCherry-Clover (Figure 1D). De novo fluorophore maturation of anaerobically synthesized GFPm is faster than maturation of sfGFP under the same conditions (Iizuka *et al.*, 2011; Supplemental Figure S1A). However, in vivo maturation (which also includes protein folding) of GFPm appears to be slower than that of sfGFP, as the R_b/R_m ratio was higher for Pma1-mCherry-GFPm than for Pma1-mCherry-sfGFP (Figure 1D). The maturation kinetics of myeGFP is

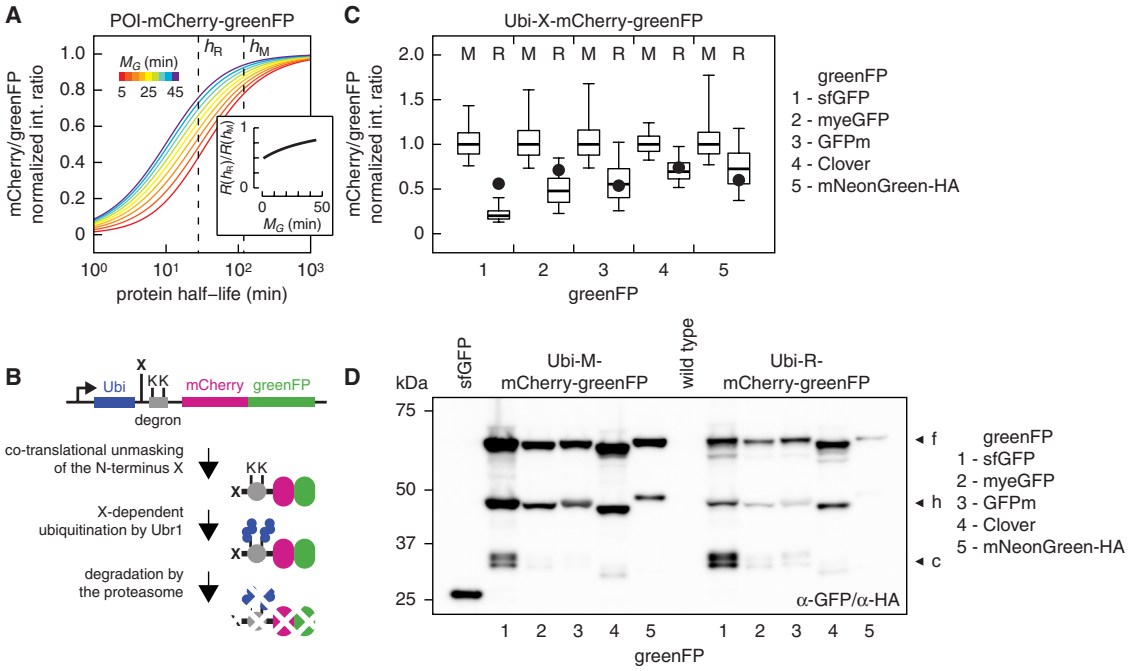

FIGURE 2: Analysis of protein degradation kinetics with different tFTs. (A) Relationship between half-life of a tFT protein fusion and mCherry/greenFP intensity ratio in steady state. mCherry/greenFP intensity ratios were calculated as a function of protein degradation kinetics for a population doubling time of 90 min using published maturation parameters for mCherry (Khmelinskii *et al.*, 2012) and a maturation half-time M_G between 5 and 45 min for greenFP. Each curve is normalized to the mCherry/greenFP intensity ratio of a nondegradable tFT fusion. Curves are color coded according to M_G as indicated. Note that protein half-life T is related to degradation rate constant k as $T = \ln(2)/k$. Similarly, maturation half-time M_G is related to maturation rate constant m_G as $M_G = \ln(2)/m_G$. Inset, comparison of mCherry/greenFP intensity ratio (R) for two protein half-lives, $h_R = 28$ min (half-life of R-mCherry-sfGFP) and $h_M = 119$ min (half-life of M-mCherry-sfGFP; Supplemental Figure S2B), as a function of M_G. (B) Cartoon of Ubi-X-mCherry-greenFP constructs. Degradation rate of X-mCherry-greenFP fusions depends on the residue X, such that X = T (slow) < M < I < Y < F < R (fast). (C) Fluorescence measurements with flow cytometry of strains expressing the indicated Ubi-X-mCherry-greenFP fusions. The residue X in each fusion is specified in the plot. Fusions with mNeonGreen carried a C-terminal HA tag to facilitate detection by immunoblotting. For each tFT, the mCherry/greenFP intensity ratios of individual cells were normalized to the median mCherry/greenFP intensity ratio of the corresponding Ubi-M-mCherry-greenFP fusion. Centerlines mark the medians, box limits indicate the 25th and 75th percentiles, and whiskers extend to 5th and 95th percentiles. Black circles mark theoretical mCherry/greenFP intensity ratios of Ubi-R-mCherry-greenFP (normalized to the corresponding Ubi-M-mCherry-greenFP fusions) calculated according to a simple model of mCherry-greenFP turnover in A using 28 and 119 min as half-lives of R-mCherry-sfGFP and M-mCherry-sfGFP, respectively, and published maturation half-times for mCherry and different greenFPs (Supplemental Figure S1A). (D) Immunoblot of strains expressing the indicated constructs. Whole-cell extracts were separated by SDS–PAGE and probed with a mixture of antibodies against GFP and the HA tag. Three major forms observed for each Ubi-X-mCherry-greenFP fusion are indicated: a full-length, X-mCherry-greenFP form (f), a shorter, mCherry$^{\Delta N}$-greenFP product resulting from mCherry hydrolysis during cell extract preparation (h; Gross *et al.*, 2000), and fast-migrating, processed tFT fragments (c).

not known. The R_b/R_m ratio of Pma1-mCherry-myeGFP was lower than expected for a greenFP with a maturation half-time of 25 min (i.e., the maturation half-time of enhanced GFP [EGFP]; Supplemental Figure S1A; Shaner *et al.*, 2007), indicating that myeGFP matures faster than EGFP but slower than sfGFP in yeast (Figure 1D).

We proceeded to examine the performance of all tFTs as reporters of protein degradation kinetics. In steady state, the mCherry/greenFP intensity ratio is determined by the degradation kinetics of the tFT fusion, such that strains expressing rapidly degraded fusions are expected to exhibit lower mCherry/greenFP intensity ratios (Figure 2A; Khmelinskii *et al.*, 2012). We generated two constructs for expression of N-terminal ubiquitin (Ubi) fusions with each tFT (Ubi-X-mCherry-greenFP): one with a methionine residue (M) and another with an arginine residue (R) at position X (Figure 2B). Cotranslational cleavage of the ubiquitin moiety exposes a new N-terminus starting with residue X, which determines the stability of the fusion according to the N-end rule. Fusions with N-terminal arginine, but not with N-terminal methionine, are recognized by the E3 ubiquitin ligase Ubr1 and targeted for proteasomal degradation (Bachmair *et al.*, 1986; Varshavsky, 2011; Supplemental Figure S2, A and B). Accordingly, for each tFT, the mCherry/greenFP intensity ratio was lower for the strain expressing Ubi-R-mCherry-greenFP (Figure 2C), indicating that all tested tFTs report on protein degradation kinetics.

The difference between the median mCherry/greenFP intensity ratios of strains expressing Ubi-M-mCherry-greenFP and Ubi-R-mCherry-greenFP fusions varied from ~5-fold for the mCherry-sfGFP timer to 1.4- to 2.1-fold for the other tFTs. Comparison of these differences to an approximate model of tFT turnover (Figure 2A and Supplemental Theory) revealed several inconsistencies between theory and experiment. For instance, the relative mCherry/greenFP intensity ratio of Ubi-R-mCherry-sfGFP was considerably

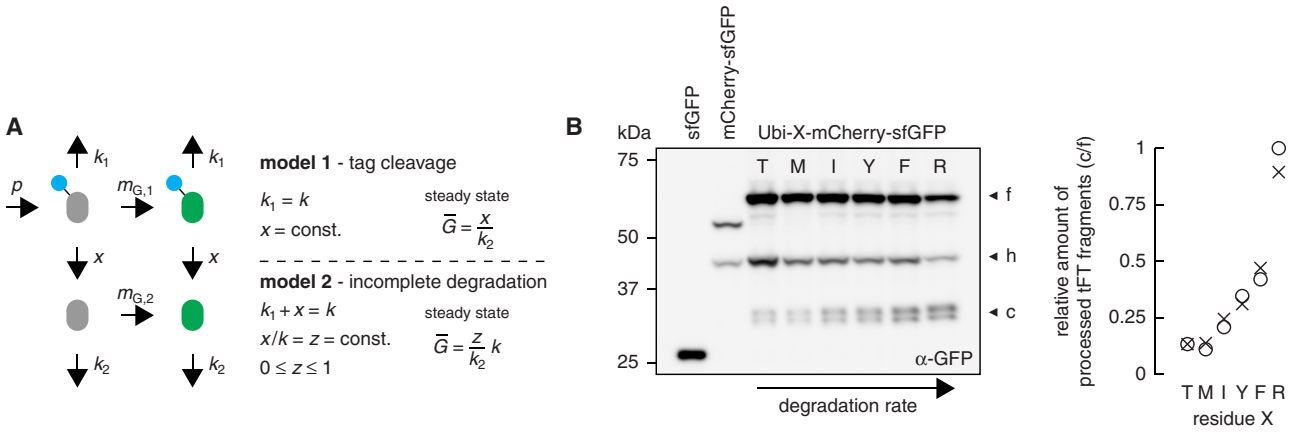

FIGURE 3: Incomplete degradation of tFT fusions leads to accumulation of processed tFT fragments. (A) Turnover of a greenFP protein fusion with accumulation of processed greenFP. We assume that a greenFP protein fusion (protein of interest, represented by a blue circle, tagged with a greenFP) is produced at a constant rate p as a nonfluorescent protein and matures to a fluorescent protein in a single step with maturation rate constant $m_{G,1}$. In model 1, greenFP protein fusions are degraded with rate constant k, and greenFP can be cleaved off from both nonmature and mature protein fusions with rate constant x. In model 2, degradation of greenFP protein fusions with rate constant k proceeds to completion with probability $1 - z$, such that greenFP fusions are effectively degraded with rate constant $k_1 = (1 - z)k$ and processed greenFP is produced with rate constant $x = kz$. Processed nonfluorescent greenFP matures in a single step with maturation rate constant $m_{G,2}$ and is degraded with rate constant k_2 in both models. In steady state, the fraction of processed greenFP ($\overline{G}$, defined as the ratio between the total number of processed greenFP molecules and the total number of greenFP protein fusion molecules) is independent of k in model 1. However, $\overline{G}$ is proportional to k in model 2. Further details are provided in Supplemental Theory. (B) Immunoblot of strains expressing the indicated constructs. The residue X in each Ubi-X-mCherry-sfGFP fusion is specified in the immunoblot. Three major forms observed for each Ubi-X-mCherry-sfGFP fusion are indicated as in Figure 2D. Note that in agreement with their degradation-dependent origin, processed tFT fragments were not detected in the strain expressing the stable mCherry-sfGFP fusion. Right, ratio between the intensities of the c and f bands measured for each strain in two independent immunoblots, normalized to the maximum c/f ratio.

lower than expected (Figure 2C). Moreover, tFTs with Clover and mNeonGreen exhibited similar relative mCherry/greenFP intensity ratios for Ubi-R-mCherry-greenFP (Figure 2C), despite the difference in maturation kinetics (Supplemental Figure S1A) and distinct performance as reporters of protein age (Figure 1D). These observations suggest that a parameter other than greenFP maturation kinetics influences tFT behavior in the protein degradation assay. Immunoblotting of whole-cell extracts with antibodies against GFP (or against a hemagglutinin [HA] epitope fused to the C-terminus of mNeonGreen) revealed several bands in addition to full-length fusions. The band at ~45 kDa (band h in Figure 2D) is explained by hydrolysis of the mature mCherry fluorophore during cell extract preparation, which leads to a break in the mCherry polypeptide (Gross *et al.*, 2000; Shemiakina *et al.*, 2012). In addition, unexpected tFT fragments were detected around 33 kDa (~6 kDa larger than free greenFP) in all strains expressing Ubi-X-mCherry-greenFP fusions (band c in Figure 2D). These fragments were most prominently seen for the tFT with sfGFP, especially for the Ubi-R-mCherry-sfGFP fusion. We sought to determine the origin of these protein fragments (hereafter referred to as processed tFT fragments) and examine whether their presence can account for the unexpected behavior of different tFTs.

Two mechanisms could generate processed tFT fragments: proteolytic cleavage of the tFT by an endopeptidase (model 1) and incomplete degradation of the tFT by the proteasome (model 2; Figure 3A). In model 1, the fraction of processed tFT in steady state ($\overline{G}$) is expected to be independent of the degradation kinetics of the tFT fusion. In contrast, $\overline{G}$ is expected to be proportional to the degradation kinetics of the tFT fusion in model 2 (further details in the Supplemental Theory). In both models, processed tFT fragments accumulate only if their degradation rate constant (k_2 in Figure 3A) is small. Immunoblotting analysis of strains expressing a series of Ubi-X-mCherry-sfGFP fusions with different stabilities showed that the fraction of processed tFT increases as a function of protein degradation kinetics, in agreement with model 2 (Figure 3B). Moreover, accumulation of processed tFT fragments depended on proteasomal activity (Supplemental Figure S2C). These observations were not specific to the Ubi-X-mCherry-greenFP fusions. Processed tFT fragments could also be detected in strains expressing misfolded cytoplasmic proteins tagged with mCherry-sfGFP, and the fraction of processed tFT decreased upon deletion of E3 ubiquitin ligases involved in degradation of these misfolded proteins (Supplemental Figure S2, D and E). Finally, similar ~33-kDa fragments are observed when GFP fusions are degraded by proteasomes with impaired processivity, for example, in mutants of the proteasome-associated E3 ubiquitin ligase Hul5 (or its mammalian orthologue, UBE3C; Zhang and Coffino, 2004; Aviram and Kornitzer, 2010; Martínez-Noël *et al.*, 2012; Chu *et al.*, 2013). We conclude that accumulation of processed tFT fragments is caused by incomplete proteasomal degradation of tFT fusions and that these fragments appear to be relatively stable in the cell.

What features of the mCherry-sfGFP timer are responsible for its incomplete degradation? We considered two possibilities: the linker connecting mCherry to sfGFP and the robust fold of sfGFP. The linker between mCherry and greenFP in the tFTs is composed of a leucine (L) and an aspartate (D) residue, followed by five glycine–alanine (GA) repeats (LD(GA)$_5$). GA-rich sequences can prevent complete protein degradation by impairing the ability of the proteasome to unfold its substrate (Hoyt *et al.*, 2006; Daskalogianni *et al.*, 2008). To determine the role of the linker in the accumulation of

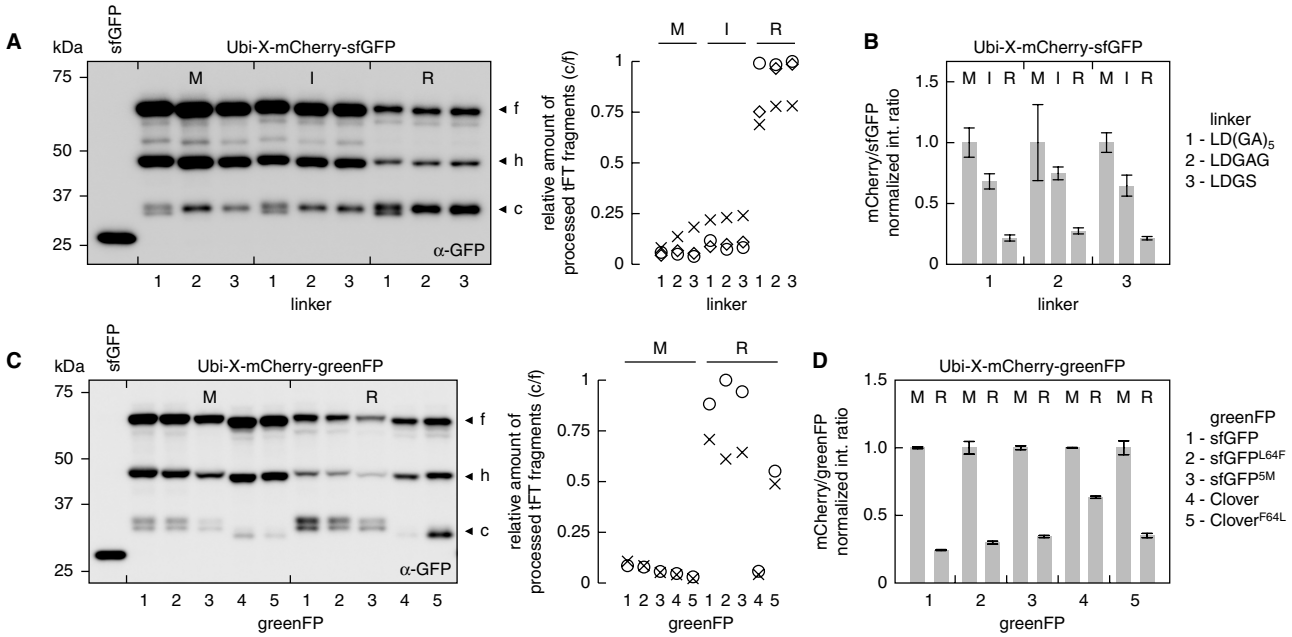

FIGURE 4: Stable greenFP fold prevents complete degradation of tFT fusions. (A) Immunoblot of strains expressing Ubi-X-mCherry-sfGFP constructs with the indicated linkers between mCherry and sfGFP. The residue X in each Ubi-X-mCherry-sfGFP fusion is specified in the immunoblot. Whole-cell extracts were separated by SDS–PAGE and probed with antibodies against GFP. Three major forms observed for each Ubi-X-mCherry-sfGFP fusion are indicated as in Figure 2D. Right, ratio between the intensities of the c and f bands measured for each strain in three independent immunoblots, normalized to the maximum c/f ratio. (B) mCherry/sfGFP intensity ratios determined from whole-colony fluorescence measurements of strains expressing Ubi-X-mCherry-sfGFP constructs in A. For each linker, mCherry/sfGFP intensity ratios (mean ± SD, $n \geq 12$ per construct) were normalized to the corresponding Ubi-M-mCherry-sfGFP fusion. (C) Immunoblot of strains expressing Ubi-X-mCherry-greenFP constructs with the indicated greenFPs. The residue X in each Ubi-X-mCherry-greenFP fusion is specified in the immunoblot. Three major forms observed for each fusion are indicated as in Figure 2D. Right, ratio between the intensities of the c and f bands measured for each strain in two independent immunoblots, normalized to the maximum c/f ratio. (D) mCherry/greenFP intensity ratios determined from whole-colony fluorescence measurements of strains expressing Ubi-X-mCherry-greenFP constructs in C. For each greenFP, mCherry/greenFP intensity ratios (mean ± SD, $n \geq 4$ per construct) were normalized to the corresponding Ubi-M-mCherry-greenFP fusion.

processed tFT fragments, we tested shorter LDGAG or LDGS linker sequences between mCherry and sfGFP. Although shorter linkers changed the relative amounts of different processed tFT fragments, they did not reduce the total amount of processed fragments (Figure 4A) or alter the ability of the mCherry-sfGFP timer to report on protein degradation kinetics (Figure 4B). In contrast, exchanging sfGFP for other greenFPs while keeping the $LD(GA)_5$ linker between mCherry and greenFP constant reduced the amount of processed tFT fragments (Figure 2D). Moreover, fragments resulting from incomplete proteasomal degradation could be detected when using sfGFP but not mCherry alone as a tag (Supplemental Figure S2F). This suggests that the stability of the greenFP fold, not the linker, is responsible for incomplete degradation of tFT fusions, although we cannot exclude the possibility that processed tFT fragments from timers other than mCherry-sfGFP are rapidly degraded in the cell.

To test the possibility that incomplete degradation is caused by the robust fold of sfGFP, we attempted to destabilize the sfGFP fold by reverting five mutations (S30R, Y39N, N105T, Y145F, and I171V) responsible for the superfolder nature of sfGFP (Pédelacq *et al.*, 2006; $sfGFP^{5M}$) or reverting the F64L mutation known to improve GFP folding at 37°C (Cormack *et al.*, 1996; Tsien, 1998; $sfGFP^{L64F}$). However, tFTs with these sfGFP mutants behaved similarly to the mCherry-sfGFP timer (Figure 4, C and D). Nevertheless, in a reverse experiment, introducing the F64L mutation into Clover increased the accumulation of processed tFT fragments in the strain expressing Ubi-R-mCherry-$Clover^{F64L}$ (Figure 4C). This accumulation correlated with a reduced mCherry/greenFP intensity ratio of Ubi-R-mCherry-$Clover^{F64L}$ relative to the Ubi-M-mCherry-$Clover^{F64L}$ fusion, bringing it close to Ubi-R-mCherry-sfGFP (Figure 4D). The F64L mutation did not affect the accumulation of processed tFT fragments for the Ubi-M-mCherry-$Clover^{F64L}$ fusion, possibly because the longer half-life of Ubi-M-tFT fusions gives enough time for complete folding and maturation of wild-type Clover. These observations support the idea that the stability of the greenFP fold is responsible for incomplete degradation of tFT fusions.

Next we sought to destabilize the sfGFP fold through circular permutations. Circular permutation can drastically impair folding of classical GFP (Baird *et al.*, 1999; Topell *et al.*, 1999). Although sfGFP is largely tolerant of circular permutations (Pédelacq *et al.*, 2006), some circularly permutated sfGFP variants can be efficiently unfolded and more rapidly degraded by the AAA+ ClpXP protease in vitro (Nager *et al.*, 2011). We constructed a series of tFTs with different circular permutations (cp's) of sfGFP (Figure 5A) and examined their behavior in the degradation assay with N-terminal ubiquitin fusions. Accumulation of processed tFT fragments was reduced to below the detection limit with all circular permutations except cp3 (Figure 5B). This is consistent with higher mobility of the β_7-β_{11} sheets in the β-barrel fold and the tendency of GFP to start unfolding from β_7-β_{11} (Huang *et al.*, 2007; Zimmer *et al.*, 2014). As seen in the case of Clover (Figure 4, C and D), reduced accumulation of processed tFT

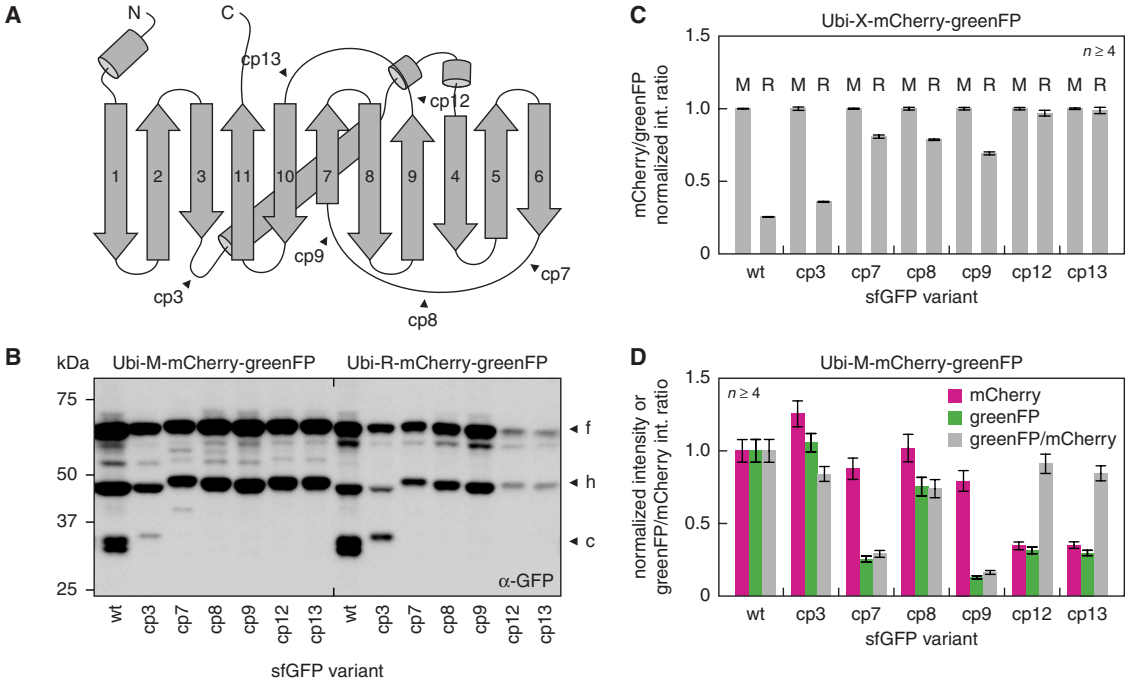

FIGURE 5: Improved degradation of tFT fusions with circular permutations of sfGFP. (A) Schematic representation of sfGFP. Start sites of six circular permutations (cp's) are indicated, numbered according to Pédelacq *et al.* (2006). (B) Immunoblot of strains expressing Ubi-X-mCherry-greenFP constructs with different circular permutations of sfGFP as greenFP. Three major forms observed for each fusion are indicated as in Figure 2D. (C, D) Whole-colony fluorescence measurements of strains expressing Ubi-X-mCherry-greenFP constructs in B. (C) The residue X in each fusion is specified in the plot. For each sfGFP variant, mCherry/greenFP intensity ratios (mean ± SD, $n \geq 4$ per construct) were normalized to the corresponding Ubi-M-mCherry-greenFP fusion. (D) mCherry fluorescence intensities (measure of expression levels), greenFP fluorescence intensities, and greenFP/mCherry intensity ratios (measure of greenFP molecular brightness; mean ± SD, $n \geq 4$ per construct) were normalized to Ubi-M-mCherry-sfGFP.

fragments correlated with reduced relative difference in mCherry/greenFP ratios between stable and unstable Ubi-X-mCherry-greenFP fusions (Figure 5C). Taken together, these experiments indicate that the stability of the greenFP fold is responsible for proteasome-dependent processing of tFTs and concomitant accumulation of tFT fragments.

Two permutations, cp7 and cp9, reduced the molecular brightness of sfGFP (Figure 5D). Another two, cp12 and cp13, appeared to affect protein folding and expression levels (Figure 5D) and the maturation kinetics of sfGFP, as suggested by the lack of difference in mCherry/sfGFP ratios between the two Ubi-X-mCherry-greenFP fusions (Figure 5C). However, the cp8 permutation did not impair protein expression and had only a minor effect on the molecular brightness of sfGFP (Figure 5D). sfGFP(cp8) exhibited the fastest maturation kinetics among all tested circular permutations, as evidenced by the performance of the mCherry-sfGFP(cp8) timer in the analysis of Pma1 protein age (Figure 1D). Moreover, accumulation of processed tFT fragments was strongly reduced in human embryonic kidney HEK293T cells when using the mCherry-sfGFP(cp8) timer instead of mCherry-sfGFP (Supplemental Figure S3). Thus sfGFP(cp8) represents an alternative to sfGFP without potential artifacts caused by incomplete proteasomal degradation.

We sought to determine how incomplete proteasomal degradation affects the properties of tFTs and their use in studies of protein dynamics. We incorporated proteasome-dependent processing into a model of tFT maturation and turnover for two tFTs, mCherry-sfGFP and sfGFP-mCherry. Proteasomal degradation typically requires an unstructured region in the substrate to initiate degradation (Prakash *et al.*, 2004). We assumed that no such initiation region is present in the mCherry-sfGFP and sfGFP-mCherry timers. It is implicit in the model that degradation is initiated within the tagged protein of interest and proceeds in a processive manner until the sfGFP fold is reached, at which point the remaining polypeptide can be either released from the proteasome with a defined probability or completely degraded. Incomplete degradation of proteins tagged at the C-terminus with mCherry-sfGFP or sfGFP-mCherry produces free sfGFP or free sfGFP-mCherry, respectively, in the model (for further details, see Supplemental Theory). Our experiments indicate that the mCherry-sfGFP timer functions as a degradation reporter with C-terminally tagged proteins (Figure 2; Khmelinskii *et al.*, 2012). However, the time range of this timer shifts toward more stable proteins when the probability of incomplete tFT degradation is increased in the model (Figures 6A). This shift does not depend on whether Förster resonance energy transfer (FRET) from sfGFP to mCherry is considered in the model (Supplemental Theory and Supplemental Figure S4). The difference in mCherry/sfGFP intensity ratios between Ubi-M-mCherry-sfGFP and Ubi-R-mCherry-sfGFP fusions is expected to increase with increasing probability of incomplete tFT degradation (Figure 6A). The experimentally observed behavior of Clover- and sfGFP-based tFTs with different levels of incomplete tFT degradation is consistent with this prediction (Figures 4D and 5C).

In contrast to the mCherry-sfGFP timer, incomplete degradation of the sfGFP-mCherry timer as a C-terminal tag is predicted to abolish the monotonic relationship between mCherry/sfGFP intensity ratio and protein half-life (Figure 6B). We tested this prediction in the

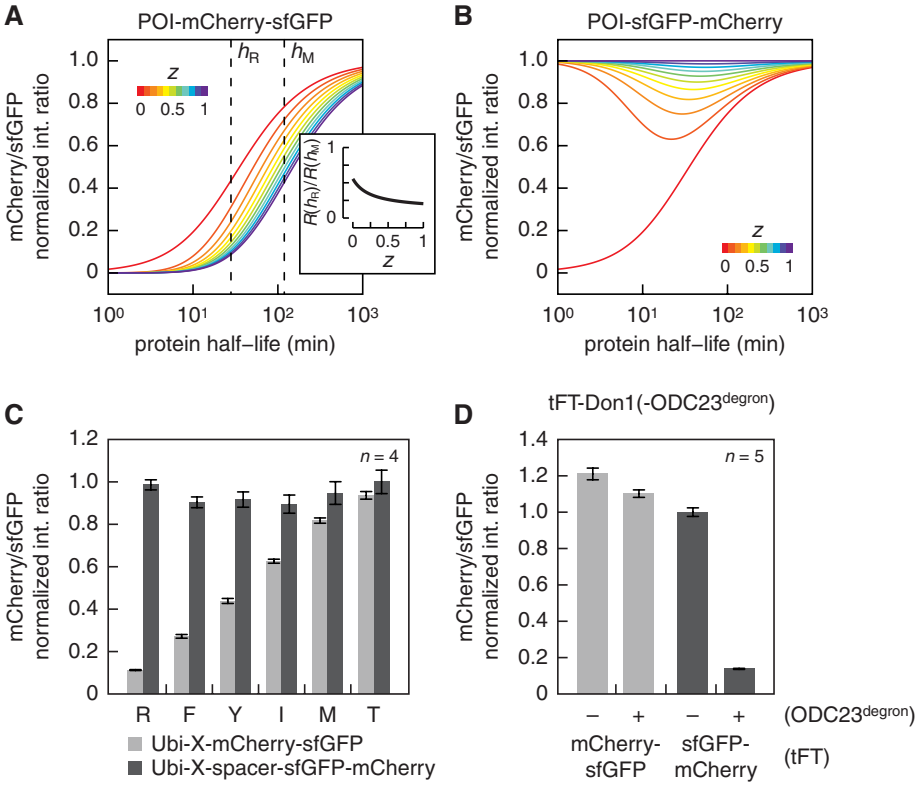

FIGURE 6: Proteasome-dependent processing constrains the design of tFTs. (A, B) Relationship between half-life of a protein of interest (POI) tagged at the C-terminus with a tFT and mCherry/sfGFP intensity ratio in steady state. mCherry/sfGFP intensity ratios were calculated as a function of protein degradation kinetics for a population doubling time of 90 min using published maturation parameters for mCherry and sfGFP (Khmelinskii *et al.*, 2012) and a probability *z* of incomplete degradation of sfGFP between 0 and 1. Incomplete degradation produces free sfGFP in A or free sfGFP-mCherry in B. Each curve is normalized to the mCherry/sfGFP intensity ratio of a nondegradable tFT fusion. Curves are color coded according to *z* as indicated. Further details are provided in Supplemental Theory. Inset, comparison of mCherry/sfGFP intensity ratio (*R*) for two protein half-lives, h_R = 28 min (half-life of R-mCherry-sfGFP) and h_M = 119 min (half-life of M-mCherry-sfGFP; Supplemental Figure S2B), as a function of *z*. (C) Fluorescence measurements with flow cytometry of strains expressing the indicated Ubi-X-tFT fusions. The residue X in each fusion is specified in the plot. mCherry/sfGFP intensity ratios (mean ± SD, *n* = 4 per construct) were normalized to Ubi-T-spacer-sfGFP-mCherry. (D) Whole-colony fluorescence measurements of strains expressing tFT-Don1 fusions with and without an ODC23 degron at the C-terminus. The tFT in each fusion is specified in the plot. mCherry/sfGFP intensity ratios (mean ± SD, *n* = 5 per construct) were normalized to sfGFP-mCherry-Don1.

degradation assay with N-terminal ubiquitin fusions. To ensure initiation of degradation N-terminally to sfGFP, we separated the N-terminal degradation signal (N-degron) from the sfGFP-mCherry timer with a spacer protein Don1 and an HA tag (Ubi-X-spacer-sfGFP-mCherry). Immunoblotting of whole-cell extracts confirmed the accumulation of processed tFT fragments with the expected size, ~6 kDa larger than free sfGFP-mCherry, in these strains (Supplemental Figure S5A). In contrast to strains expressing Ubi-X-mCherry-sfGFP fusions, the mCherry/sfGFP intensity ratio was largely independent of the degradation rate for Ubi-X-spacer-sfGFP-mCherry fusions (Figure 6C and Supplemental Figure S5B). This result is consistent with the model predictions and suggests that the probability of incomplete sfGFP degradation is substantial (~0.5 or higher; Figure 6B). Moreover, it shows that the sfGFP-mCherry timer should not be used as a degradation reporter with C-terminally tagged proteins. However, it is important to stress that the sfGFP-mCherry fusion is a timer, that is, it changes color with time, and thus should report on the age of C-terminally tagged proteins in the absence of protein degradation. Indeed, cells expressing Pma1-sfGFP-mCherry exhibited lower mCherry/sfGFP intensity ratios at the plasma membrane in the bud than in the mother cell, similarly to Pma1-mCherry-sfGFP (Figure 1D). Moreover, the sfGFP-mCherry timer, but not the mCherry-sfGFP timer, faithfully reported on the degradation kinetics of N-terminally tagged proteins (Figure 6D and Supplemental Figure S5C). Together these results indicate that different tFT variants should be used for N- and C-terminal protein tagging, such that the sfGFP moiety is placed distally to the region in the protein of interest where proteasomal degradation is initiated. Of importance, this theoretical analysis was performed under the assumption that processed tFT fragments are stable in the cell (Figure 6, A and B) and thus establishes an upper limit for the influence of proteasome-dependent processing of tFTs on their ability to report on protein degradation kinetics. Increasing the degradation rate of processed tFT fragments reduces their impact and, at the limit of infinitely fast degradation, mCherry-sfGFP and sfGFP-mCherry timers are both reporters of protein degradation kinetics when used for C-terminal tagging, with behavior indistinguishable from that of a hypothetical mCherry-sfGFP timer that is completely degraded by the proteasome (Supplemental Theory and Supplemental Figure S6).

DISCUSSION

We report here on the use of different greenFPs for analysis of protein dynamics with tFTs. All tested greenFPs can be combined with mCherry to obtain tFTs that report on protein age and degradation kinetics, indicating that greenFPs mature faster than mCherry. Our analysis shows that the greenFP maturation kinetics influences the time range of mCherry-greenFP timers (Figure 1). In addition, we observe that greenFPs (especially sfGFP), but not mCherry, can withstand proteasomal degradation in yeast (Figure 2 and Supplemental Figure S2F), consistent with previous reports of incomplete proteasomal degradation of GFP (Zhang and Coffino, 2004; Aviram and Kornitzer, 2010; Martínez-Noël *et al.*, 2012; Chu *et al.*, 2013). The efficiency of FP degradation by the proteasome could differ in other organisms and cell types, as proteasome processivity varies among species (Kraut *et al.*, 2012).

Two features are necessary for a protein to become a proteasome substrate: a degradation signal (degron) and a degradation initiation site (Schrader *et al.*, 2009). These features are provided by the model substrates used to investigate tFT behavior in the degradation assay (Figure 2). Therefore, proteasomal degradation of a tFT starts from the site where it is linked to the model substrate and proceeds by unfolding and channeling of the polypeptide into the catalytic core of the 19S particle of the proteasome. Protein sequences that cannot be efficiently channeled into the

catalytic core can be release from the proteasome. Several factors can contribute to this release: the protein sequence adjacent to the released domain, the stability of the fold of the released domain, and an intrinsic probability of the proteasome to release substrates that is independent of the power stroke underlying substrate unfolding (Kraut *et al.*, 2012; Fishbain *et al.*, 2015). Our analysis indicates that incomplete degradation of sfGFP fusions depends on the stability of the sfGFP fold (Figures 4 and 5), although the molecular details, that is, the determinants in sfGFP, are unclear.

The outcome of proteasomal processing of tFT fusions depends on the order of FPs in the timer relative to the region in the protein from which proteasomal degradation begins. If mCherry is placed proximal to the degradation initiation site (e.g., in the mCherry-sfGFP timer as a C-terminal tag), proteasomal processing produces tFT fragments of ~33 kDa (Figure 2). These contain the greenFP moiety and a short, ~6-kDa tail that presumably corresponds to the length of the unfolded polypeptide channeled into the proteasome catalytic core before release of the fragments. In this situation, the timer functions as a reporter of protein age and degradation kinetics, but its time range is shifted toward more stable proteins compared with a hypothetical timer that is completely degraded by the proteasome (Figure 6A). This shift should increase the difference in mCherry/greenFP intensity ratios between the stable Ubi-M-tFT and unstable Ubi-R-tFT fusions (inset in Figure 6A), as experimentally observed for the mCherry-sfGFP timer compared with mCherry-sfGFP(cp8) or mCherry-mNeonGreen (Figures 2C and 5C). Moreover, the increased cytoplasmic greenFP fluorescence resulting from incomplete tFT degradation should be taken into account when measuring protein age at subcellular level. We note that the ~33-kDa tFT fragments are distinct from the ~26-kDa fragments observed upon incomplete lysosomal/vacuolar degradation of GFP fusions, which have been exploited to follow the cytoplasm-to-vacuole targeting pathway and autophagy (Shintani and Klionsky, 2004; Klionsky *et al.*, 2008). If in turn greenFP is located proximal to the degradation initiation site (e.g., in the sfGFP-mCherry timer as a C-terminal tag), proteasomal processing results in the release of ~60-kDa tFT fragments containing both FPs and a short, ~6-kDa tail (Supplemental Figure S5A). In this case, the timer can be still used to measure local protein age, but it no longer reports on protein degradation kinetics (Figure 6B). From these observations, we can derive the following list of recommendations for design and use of tFTs as reporters of protein age and degradation.

1. The time range of a tFT is mostly determined by the maturation kinetics of the slower-maturing FP (Khmelinskii *et al.*, 2012), although the maturation kinetics of the faster-maturing FP, the extent of proteasomal processing, and potential FRET between the two FPs also contribute (Figures 2A and 6A and Supplemental Figure S4A). Thus, to construct a tFT for a given time range, a slower-maturing FP with maturation kinetics matching the time scale of interest should be paired with a faster-maturing FP that is as bright and fast maturing as possible to lower the detection limit of the timer (Khmelinskii and Knop, 2014).
2. Ideally, characterization of a new tFT should involve testing both arrangements of FPs as reporters of protein age and protein degradation in the experimental system of interest to obtain qualitative system-specific estimates of FP maturation rates, efficiency of proteasomal degradation, and time range of the tFT. In yeast, this can be done using the Pma1 protein age and Ubi-X-tFT degradation assays (Figures 1D and 2C).
3. For tFTs based on mCherry and greenFPs (or any timer in which one of the FPs is resistant to proteasomal degradation), the FPs should be arranged such that the degradation-resistant greenFP ends up distal to the degradation initiation site in the tagged protein of interest. Thus the mCherry-sfGFP timer should be used for C-terminal tagging and the sfGFP-mCherry timer for N-terminal tagging. For internal tagging, both timers should be tested to first identify the degradation initiation site based on the size of processed tFT fragments.
4. Generally, a tFT in which both FPs are efficiently degraded by the proteasome is preferable, assuming its time range is suitable for the intended analysis. However, tFTs with incomplete proteasomal degradation can be advantageous in some situations. For instance, although the time range of mCherry-sfGFP(cp8) and mCherry-mNeonGreen timers is in principle more suitable to studying degradation of unstable proteins than mCherry-sfGFP (Figure 6A), the mCherry-sfGFP timer could facilitate detection of extremely unstable and low-abundance proteins due to increased absolute greenFP fluorescence that results from accumulation of processed tFT fragments. Moreover, processed tFT fragments can be exploited as a marker of proteasomal degradation. For example, for a protein tagged at the C-terminus with mCherry-sfGFP, accumulation of ~33-kDa fragments is indicative of proteasomal degradation (Supplemental Figure S2C), whereas lysosomal/vacuolar degradation should produce ~26-kDa fragments (Shintani and Klionsky, 2004; Klionsky *et al.*, 2008).
5. tFTs with incomplete proteasomal degradation such as mCherry-sfGFP can be used for systematic analysis of protein degradation, as the mCherry/sfGFP intensity ratio in steady state is a monotonic function of protein half-life (Figure 6A). However, care should be exercised when comparing proteins degraded by the proteasome and lysosome/vacuole pathways, which produce distinct tFT degradation fragments and differ in local environment that can affect FP maturation and brightness (Khmelinskii and Knop, 2014).

To follow protein dynamics, fast-maturing FP tags are needed to detect proteins as early as possible after synthesis. Our analysis indicates that mNeonGreen (Lam *et al.*, 2012) is a good alternative to sfGFP: it is similarly fast maturing but significantly less resistant to proteasomal degradation in yeast than sfGFP (Figures 1 and 2). The molecular brightness of mNeonGreen is similar to that of sfGFP when using excitation/emission wavelengths optimal for sfGFP and approximately five times higher with wavelengths optimal for mNeonGreen (Supplemental Figure S1). The only limitation is that filter sets matching the excitation/emission peaks of mNeonGreen or lasers around its 506-nm excitation peak are not commonly used in fluorescence microscopy. The cp8 circular permutation of sfGFP is another alternative. When used as a C-terminal tag, sfGFP(cp8) is completely degraded by the proteasome in both yeast and human cells, and its maturation kinetics and brightness are similar to those of sfGFP (Figure 5 and Supplemental Figure S3).

In conclusion, our study provides a detailed characterization of tFTs as reporters of protein age and degradation. This should facilitate their application in different areas of cellular and organismal research. Our work also emphasizes the notion that fluorescent proteins are not neutral tags. Careful characterization of their properties is required for correct interpretation of protein dynamics measurements across spatial and temporal dimensions.

MATERIALS AND METHODS

Yeast methods and plasmids

Yeast genome manipulations (gene deletions and tagging) were performed using conventional PCR targeting, as described (Janke *et al.*, 2004). Yeast strains and plasmids used in this study are listed in Supplemental Tables S1 and S2, respectively. Yeast codon-optimized sequences of all fluorescent proteins were obtained using full gene synthesis. All Ubi-X-tFT constructs are based on previously described Ubi-X-β-galactosidase fusions, where X is followed by a 40-residue sequence that starts with histidine (Bachmair *et al.*, 1986). The sequence of the ubiquitin-independent ODC23 degron (MSCAQESITSLYKKAGSENLYFQ) was obtained from plasmid pCT334 (Renicke *et al.*, 2013). The Don1 coding sequence was amplified from genomic DNA of strain ESM356-1 (Supplemental Table S1). Standard site-directed mutagenesis was used to introduce point mutations into sfGFP or Clover and change the linker between mCherry and sfGFP. Circular permutations of sfGFP were amplified from a plasmid carrying two copies of sfGFP fused with a short linker (GSGAG). The N-termini of circular permutations 3, 7, 8, 9, 12, and 13 are the amino acids at positions 51, 129, 140, 145, 189, and 189 of sfGFP, respectively. All plasmid sequences are available upon request.

Models of tFT maturation and turnover

Fluorescence intensity curves depicting maturation of a pool of mCherry-sfGFP molecules initialized in the nonmature state in the absence of protein production and degradation (Figure 1A) were calculated using a two-step maturation model for mCherry (maturation half-times of 16.91 and 30.3 min) and a one-step maturation model for sfGFP (maturation half-time of 5.63 min), as described (Khmelinskii *et al.*, 2012). To examine the influence of greenFP on tFT maturation (Figure 1B), the maturation half-time of greenFP was varied between 5 and 45 min in 5-min steps. All curves were normalized to the point of complete maturation.

To examine the influence of greenFP maturation on the relationship between protein half-life and mCherry/greenFP intensity ratio in steady state (Figure 2A), mCherry/greenFP intensity ratios were calculated according to Eq. E33 in the Supplemental Theory, using a probability of incomplete tFT degradation $z = 0$, mCherry maturation half-times of 16.91 and 30.3 min, greenFP maturation half-time between 5 and 45 min varied in 5-min steps and a population doubling time of 90 min.

To examine the influence of incomplete tFT degradation on the relationship between protein half-life and mCherry/sfGFP intensity ratio in steady state (Figure 6, A and B), mCherry/sfGFP intensity ratios were calculated for the mCherry-sfGFP and sfGFP-mCherry timers according to Eqs. E33 and E34, respectively, of the Supplemental Theory, using a population doubling time of 90 min, mCherry maturation half-times of 16.91 and 30.3 min for both full-length fusion and processed forms, sfGFP maturation half-time of 5.63 min for both full-length fusion and processed forms, a degradation rate constant of processed tFT fragments $k_2 = 0$, and varied probability of incomplete tFT degradation z between 0 and 1 in steps of 0.1.

To examine the influence of FRET within a tFT on the relationship between protein half-life and mCherry/sfGFP intensity ratio in steady state (Supplemental Figure S4A), mCherry/sfGFP intensity ratios were calculated for the mCherry-sfGFP timer according to Eq. E39 of the Supplemental Theory, using a population doubling time of 90 min, a probability of incomplete tFT degradation $z = 0$, mCherry maturation half-times of 16.91 and 30.3 min, sfGFP maturation half-time of 5.63 min, and varied FRET efficiency E between 0 and 1 in steps of 0.1. For a fixed FRET efficiency E (0, 0.5, or 1; Supplemental Figure S4, B–D), the calculations were extended by varying the probability of incomplete tFT degradation z between 0 and 1 in steps of 0.1, using a degradation rate constant of processed tFT fragments $k_2 = 0$ and sfGFP maturation half-time of 5.63 min for both full-length fusion and processed forms.

To examine how degradation of processed tFT fragments influences the relationship between protein half-life and mCherry/sfGFP intensity ratio in steady state (Supplemental Figure S6), mCherry/sfGFP intensity ratios were calculated for the mCherry-sfGFP and sfGFP-mCherry timers according to Eqs. E33 and E34, respectively, of the Supplemental Theory, using a population doubling time of 90 min, mCherry maturation half-times of 16.91 and 30.3 min for both full-length fusion and processed forms, sfGFP maturation half-time of 5.63 min for both full-length fusion and processed forms, a probability of incomplete tFT degradation $z = 1$, and varied the half-life of processed tFT fragments H_2 between 10 and 1000 min, in addition to 0 and ∞. The half-life of processed tFT fragments H_2 is related to the degradation rate constant of processed tFT fragments k_2 as $k_2 = \ln(2)/H_2$.

Fluorescence microscopy

Strains were grown at 30°C in low-fluorescence medium (synthetic complete medium prepared with yeast nitrogen base lacking folic acid and riboflavin [CYN6501; ForMedium, Hunstanton, UK]) to $(0.4–1.2) \times 10^7$ cells/ml and attached to glass-bottom 96-well plates (MGB096-1-2-LG-L; Brooks Life Science Systems, Spokane, WA) using concanavalin A (C7275; Sigma-Aldrich, Steinheim, Germany) as described (Khmelinskii and Knop, 2014). Images from the middle of the cell were acquired on a DeltaVision Elite system (GE Healthcare Life Sciences, Freiburg, Germany), consisting of an inverted epifluorescence microscope (IX71; Olympus, Hamburg, Germany) equipped with an LED light engine (SpectraX; Lumencor, Beaverton, OR), 475/28- and 575/25-nm excitation and 525/50- and 624/40-nm emission filters (Semrock, Rochester, NY), a dual-band beam splitter 89021 (Chroma Technology, Bellows Falls, VT), a 100×/numerical aperture 1.4 UPlanSApo oil immersion objective (Olympus), a scientific CMOS camera (pco.edge 4.2; PCO, Kelheim, Germany), and a motorized stage contained in a temperature-controlled chamber. Image correction and quantification were performed using ImageJ (Schneider *et al.*, 2012). Dark-signal and flat-field corrections were applied to all images as described (Khmelinskii and Knop, 2014). Outlines of mother and bud compartments were manually defined in the sfGFP channel using a 5-pixel-wide segmented line with a spline fit and applied to the mCherry channel. Fluorescence measurements at the plasma membrane were corrected for background using autofluorescence of the growth medium measured in close proximity to each individual cell.

Flow cytometry

Strains were grown at 30°C in synthetic medium lacking leucine (to select for plasmids) to a density of $(0.4–1.2) \times 10^7$ cells/ml. Single-cell fluorescence intensities, forward and side scatter, were measured for at least 6000 cells/sample on a BD FACSCanto RUO Special Order System (BD Biosciences, Franklin Lakes, NJ) equipped with 488- and 561-nm lasers, 505- and 600-nm long-pass filters, and 530/30- and 610/20-nm band-pass filters. Multispectral beads (3.0–3.4 μm Sphero Rainbow Calibration Particles, six peaks; 556286; BD Biosciences) were used to control for fluctuations in excitation laser power. Data analysis was performed with Flowing Software 2 (www.flowingsoftware.com): measurements were gated for cells, followed by gating for cells with fluorescence above background to exclude

cells that lost the expression plasmids. Sample measurements were corrected for background using autofluorescence levels of a control strain carrying an empty plasmid. mCherry/greenFP intensity ratios were calculated for each individual cell.

Colony fluorescence measurements

Strains were grown to saturation at 30°C in synthetic medium lacking leucine and pinned onto agar plates with synthetic medium lacking leucine in 384-colony format, with four technical replicates for each strain. A RoToR pinning robot (Singer Instruments, Watchet, UK) was used for pinning. Fluorescence intensities of colonies were typically measured after 24 h of growth at 30°C using an Infinite M1000 Pro plate reader (Tecan, Männedorf, Switzerland). Measurements in mCherry (587/10-nm excitation, 610/10-nm emission, optimal detector gain) and sfGFP (488/10-nm excitation, 510/10-nm emission, optimal detector gain) channels were performed from the top at 400-Hz frequency of the flash lamp, with 20 flashes averaged for each measurement. For relative measurements of molecular brightness of different greenFPs (Supplemental Figure S1B), fluorescence intensities were additionally measured in a third channel (505/5-nm excitation, 516/5-nm emission, optimal detector gain). Measurements of control colonies without fluorescent protein expression were used to correct all measurements for background.

To acquire excitation spectra (Supplemental Figure S1C), exponentially growing cultures of strains yMaM26 and yMaM32 (Supplemental Table S1) were transferred to glass-bottom 96-well plates (MGB096-1-2-LG-L; Brooks Life Science Systems) and allowed to settle down. Fluorescence emission at 510/5 nm was measured from the bottom with excitation wavelengths between 350 and 600 nm in 2-nm steps at 400 Hz frequency of the flash lamp, with 1 flash/step.

Immunoblotting and time-course experiments

Strains were typically grown at 30°C in synthetic medium lacking leucine to 10^7 cells/ml. One-milliliter samples were mixed with 150 µl of 1.85 M NaOH and 10 µl of β-mercaptoethanol and flash frozen in liquid nitrogen. Whole-cell extracts were prepared as previously described (Knop *et al.*, 1999), separated by SDS–PAGE (NuPAGE Novex 4-12% Bis-Tris protein gels; Thermo Fisher Scientific, Waltham, MA) followed by blotting and probed with mouse anti-HA (12CA5), mouse anti-myc (9E10), rabbit anti-GFP (ab6556; Abcam, Cambridge, UK), rabbit anti–yellow fluorescent protein (Miller *et al.*, 2015), mouse anti-Pgk1 (22C5D8; Thermo Fisher Scientific), and rabbit anti-Zwf1 (Miller *et al.*, 2015) antibodies. Secondary goat anti-mouse immunoglobulin G (IgG)-horseradish peroxidase (HRP) (#115-035-003; Dianova, Hamburg, Germany) and goat anti-rabbit IgG-HRP (#111-035-003; Dianova) antibodies were used for detection. Imaging was performed on a LAS-4000 system (GE Healthcare Life Sciences) using the increment exposure routine to avoid overexposure. Image quantification was performed in ImageJ (Schneider *et al.*, 2012). All measurements were corrected for local background.

For cycloheximide chases, strains were grown at 30°C in synthetic complete medium to ~0.8×10^7 cells/ml before addition of cycloheximide to 100 µg/ml final concentration. One-milliliter samples taken at each time point were immediately mixed with 150 µl of 1.85 M NaOH and 10 µl of β-mercaptoethanol, flash frozen in liquid nitrogen, and processed for immunoblotting as detailed.

For the proteasome inhibition experiment (Supplemental Figure S2C), strains yMaM67 and yMaM957 (Supplemental Table S1) were grown at 30°C to ~0.8×10^7 cells/ml in synthetic medium lacking leucine and with raffinose (2% [wt/vol]) as carbon source. Expression of Ubi-R-mCherry-sfGFP was induced by addition of galactose (2% [wt/vol]) alongside inhibition of proteasome activity by addition of MG132 (40 mM stock in dimethyl sulfoxide [DMSO]) to 80 µg/ml final concentration or DMSO as control. Whole-cell extracts of samples collected before and after induction were prepared and analyzed by SDS–PAGE, followed by immunoblotting, as detailed.

Human cell culture and immunoblotting

The sequence encoding PARK6 was amplified from the plasmid pcDNA3.1/Pink1 (Meissner *et al.*, 2011) and cloned into the pcDNA5/mCherry-sfGFP vector (Khmelinskii *et al.*, 2012). pcDNA5/PARK6-mCherry-sfGFP(cp8) was cloned by overlap assembly PCR of a human codon-optimized sfGFP(cp8), which was obtained by full gene synthesis, into the pcDNA5/PARK6-mCherry-sfGFP background.

HEK293T cells were grown in DMEM supplemented with 10% (vol/vol) fetal bovine serum at 37°C in 5% (vol/vol) CO_2. Transient transfections were performed using 25-kDa linear polyethylenimine (Polysciences, Warrington, PA; Durocher *et al.*, 2002) and harvested 24 h later. To block mitochondrial protein import, cells were incubated for 3 h with 10 µM carbonyl cyanide *m*-chlorophenyl hydrazone (Sigma-Aldrich) before cell lysis.

Whole-cell extracts were separated by SDS–PAGE, followed by blotting onto a polyvinylidene fluoride membrane and probed with a monoclonal anti-GFP antibody (11814460001; Roche, Sigma-Aldrich). A secondary goat anti-mouse IgG-HRP antibody (sc-2005; Santa Cruz Biotechnology, Dallas, TX) was used for detection. Imaging was performed on an LAS-4000 system (GE Healthcare Life Sciences).

ACKNOWLEDGMENTS

We thank Christof Taxis for reagents and Marc Zimmer for comments on the manuscript. This work was supported by the Deutsche Forschungsgemeinschaft through the Sonderforschungsbereich 1036 (SFB1036; M.K., A.M., B.B., and M.K.L.) and the Hartmut Hoffmann-Berling International Graduate School of Molecular and Cellular Biology (C.H.).

REFERENCES

Aviram S, Kornitzer D (2010). The ubiquitin ligase Hul5 promotes proteasomal processivity. Mol Cell Biol 30, 985–994.

Bachmair A, Finley D, Varshavsky A (1986). In vivo half-life of a protein is a function of its amino-terminal residue. Science 234, 179–186.

Baird GS, Zacharias DA, Tsien RY (1999). Circular permutation and receptor insertion within green fluorescent proteins. Proc Natl Acad Sci USA 96, 11241–11246.

Chu BW, Kovary KM, Guillaume J, Chen L-C, Teruel MN, Wandless TJ (2013). The E3 ubiquitin ligase UBE3C enhances proteasome processivity by ubiquitinating partially proteolyzed substrates. J Biol Chem 288, 34575–34587.

Cormack BP, Valdivia RH, Falkow S (1996). FACS-optimized mutants of the green fluorescent protein (GFP). Gene 173, 33–38.

Daskalogianni C, Apcher S, Candeias MM, Naski N, Calvo F, Fåhraeus R (2008). Gly-Ala repeats induce position- and substrate-specific regulation of 26 S proteasome-dependent partial processing. J Biol Chem 283, 30090–30100.

Dean KM, Palmer AE (2014). Advances in fluorescence labeling strategies for dynamic cellular imaging. Nat Chem Biol 10, 512–523.

Dona E, Barry JD, Valentin G, Quirin C, Khmelinskii A, Kunze A, Durdu S, Newton LR, Fernandez-Minan A, Huber W, *et al.* (2013). Directional tissue migration through a self-generated chemokine gradient. Nature 503, 285–289.

Durocher Y, Perret S, Kamen A (2002). High-level and high-throughput recombinant protein production by transient transfection of suspension-growing human 293-EBNA1 cells. Nucleic Acids Res 30, E9.

Fishbain S, Inobe T, Israeli E, Chavali S, Yu H, Kago G, Babu MM, Matouschek A (2015). Sequence composition of disordered regions fine-tunes protein half-life. Nat Struct Mol Biol 22, 214–221.

Gross LA, Baird GS, Hoffman RC, Baldridge KK, Tsien RY (2000). The structure of the chromophore within DsRed, a red fluorescent protein from coral. Proc Natl Acad Sci USA 97, 11990–11995.
Hoyt MA, Zich J, Takeuchi J, Zhang M, Govaerts C, Coffino P (2006). Glycine-alanine repeats impair proper substrate unfolding by the proteasome. EMBO J 25, 1720–1729.
Huang J-R, Craggs TD, Christodoulou J, Jackson SE (2007). Stable intermediate states and high energy barriers in the unfolding of GFP. J Mol Biol 370, 356–371.
Iizuka R, Yamagishi-Shirasaki M, Funatsu T (2011). Kinetic study of de novo chromophore maturation of fluorescent proteins. Anal Biochem 414, 173–178.
Janke C, Magiera MM, Rathfelder N, Taxis C, Reber S, Maekawa H, Moreno-Borchart A, Doenges G, Schwob E, Schiebel E, *et al.* (2004). A versatile toolbox for PCR-based tagging of yeast genes: new fluorescent proteins, more markers and promoter substitution cassettes. Yeast 21, 947–962.
Khmelinskii A, Keller PJ, Bartosik A, Meurer M, Barry JD, Mardin BR, Kaufmann A, Trautmann S, Wachsmuth M, Pereira G, *et al.* (2012). Tandem fluorescent protein timers for in vivo analysis of protein dynamics. Nat Biotechnol 30, 708–714.
Khmelinskii A, Knop M (2014). Analysis of protein dynamics with tandem fluorescent protein timers. Methods Mol Biol 1174, 195–210.
Klionsky DJ, Abeliovich H, Agostinis P, Agrawal DK, Aliev G, Askew DS, Baba M, Baehrecke EH, Bahr BA, Ballabio A, *et al.* (2008). Guidelines for the use and interpretation of assays for monitoring autophagy in higher eukaryotes. Autophagy 4, 151–175.
Knop M, Siegers K, Pereira G, Zachariae W, Winsor B, Nasmyth K, Schiebel E (1999). Epitope tagging of yeast genes using a PCR-based strategy: more tags and improved practical routines. Yeast 15, 963–972.
Kraut DA, Israeli E, Schrader EK, Patil A, Nakai K, Nanavati D, Inobe T, Matouschek A (2012). Sequence- and species-dependence of proteasomal processivity. ACS Chem Biol 7, 1444–1453.
Lam AJ, St-Pierre F, Gong Y, Marshall JD, Cranfill PJ, Baird MA, McKeown MR, Wiedenmann J, Davidson MW, Schnitzer MJ, *et al.* (2012). Improving FRET dynamic range with bright green and red fluorescent proteins. Nat Methods 9, 1005–1012.
Malínská K, Malínský J, Opekarová M, Tanner W (2003). Visualization of protein compartmentation within the plasma membrane of living yeast cells. Mol Biol Cell 14, 4427–4436.
Martínez-Noël G, Galligan JT, Sowa ME, Arndt V, Overton TM, Harper JW, Howley PM (2012). Identification and proteomic analysis of distinct UBE3A/E6AP protein complexes. Mol Cell Biol 32, 3095–3106.
Meissner C, Lorenz H, Weihofen A, Selkoe DJ, Lemberg MK (2011). The mitochondrial intramembrane protease PARL cleaves human Pink1 to regulate Pink1 trafficking. J Neurochem 117, 856–867.
Miller SBM, Ho CT, Winkler J, Khokhrina M, Neuner A, Mohamed MY, Guilbride DL, Richter K, Lisby M, Schiebel E, *et al.* (2015). Compartment-specific aggregases direct distinct nuclear and cytoplasmic aggregate deposition. EMBO J 34, 778–797.
Nager AR, Baker TA, Sauer RT (2011). Stepwise unfolding of a β barrel protein by the AAA+ ClpXP protease. J Mol Biol 413, 4–16.
Pédelacq J-D, Cabantous S, Tran T, Terwilliger TC, Waldo GS (2006). Engineering and characterization of a superfolder green fluorescent protein. Nat Biotechnol 24, 79–88.
Prakash S, Tian L, Ratliff KS, Lehotzky RE, Matouschek A (2004). An unstructured initiation site is required for efficient proteasome-mediated degradation. Nat Struct Mol Biol 11, 830–837.
Renicke C, Schuster D, Usherenko S, Essen L-O, Taxis C (2013). A LOV2 domain-based optogenetic tool to control protein degradation and cellular function. Chem Biol 20, 619–626.
Schneider CA, Rasband WS, Eliceiri KW (2012). NIH Image to ImageJ: 25 years of image analysis. Nat Methods 9, 671–675.
Schrader EK, Harstad KG, Matouschek A (2009). Targeting proteins for degradation. Nat Chem Biol 5, 815–822.
Shaner NC, Lambert GG, Chammas A, Ni Y, Cranfill PJ, Baird MA, Sell BR, Allen JR, Day RN, Israelsson M, *et al.* (2013). A bright monomeric green fluorescent protein derived from Branchiostoma lanceolatum. Nat Methods 10, 407–409.
Shaner NC, Campbell RE, Steinbach PA, Giepmans BNG, Palmer AE, Tsien RY (2004). Improved monomeric red, orange and yellow fluorescent proteins derived from Discosoma sp. red fluorescent protein. Nat Biotechnol 22, 1567–1572.
Shaner NC, Patterson GH, Davidson MW (2007). Advances in fluorescent protein technology. J Cell Sci 120, 4247–4260.
Shaner NC, Steinbach PA, Tsien RY (2005). A guide to choosing fluorescent proteins. Nat Methods 2, 905–909.
Shemiakina II, Ermakova GV, Cranfill PJ, Baird MA, Evans RA, Souslova EA, Staroverov DB, Gorokhovatsky AY, Putintseva EV, Gorodnicheva TV, *et al.* (2012). A monomeric red fluorescent protein with low cytotoxicity. Nat Commun 3, 1204.
Shintani T, Klionsky DJ (2004). Cargo proteins facilitate the formation of transport vesicles in the cytoplasm to vacuole targeting pathway. J Biol Chem 279, 29889–29894.
Takizawa PA, DeRisi JL, Wilhelm JE, Vale RD (2000). Plasma membrane compartmentalization in yeast by messenger RNA transport and a septin diffusion barrier. Science 290, 341–344.
Thayer NH, Leverich CK, Fitzgibbon MP, Nelson ZW, Henderson KA, Gafken PR, Hsu JJ, Gottschling DE (2014). Identification of long-lived proteins retained in cells undergoing repeated asymmetric divisions. Proc Natl Acad Sci USA 111, 14019–14026.
Topell S, Hennecke J, Glockshuber R (1999). Circularly permuted variants of the green fluorescent protein. FEBS Lett 457, 283–289.
Tsien RY (1998). The green fluorescent protein. Annu Rev Biochem 67, 509–544.
Varshavsky A (2011). The N-end rule pathway and regulation by proteolysis. Protein Sci 20, 1298–1345.
Yoo TH, Link AJ, Tirrell DA (2007). Evolution of a fluorinated green fluorescent protein. Proc Natl Acad Sci USA 104, 13887–13890.
Zacharias DA, Violin JD, Newton AC, Tsien RY (2002). Partitioning of lipid-modified monomeric GFPs into membrane microdomains of live cells. Science 296, 913–916.
Zhang M, Coffino P (2004). Repeat sequence of Epstein-Barr virus-encoded nuclear antigen 1 protein interrupts proteasome substrate processing. J Biol Chem 279, 8635–8641.
Zimmer MH, Li B, Shahid RS, Peshkepija P, Zimmer M (2014). Structural consequences of chromophore formation and exploration of conserved lid residues amongst naturally occurring fluorescent proteins. Chem Phys 429, 5–11.